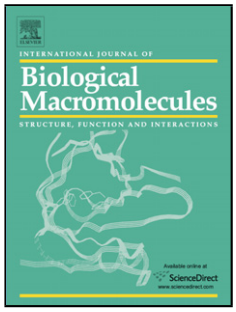

Title: Swellable Silk Fibroin Microneedles for Transdermal Drug Delivery

Authors: Zhuping Yin, Dajiang Kuang, Shiyi Wang, Zhaozhu Zheng, Vamsi K. Yadavalli, Shenzhou Lu

PII: S0141-8130(17)30939-X
DOI: http://dx.doi.org/doi:10.1016/j.ijbiomac.2017.07.178
Reference: BIOMAC 7986

To appear in: *International Journal of Biological Macromolecules*

Received date: 14-3-2017
Revised date: 28-7-2017
Accepted date: 30-7-2017

Please cite this article as: Zhuping Yin, Dajiang Kuang, Shiyi Wang, Zhaozhu Zheng, Vamsi K.Yadavalli, Shenzhou Lu, Swellable Silk Fibroin Microneedles for Transdermal Drug Delivery, International Journal of Biological Macromoleculeshttp://dx.doi.org/10.1016/j.ijbiomac.2017.07.178

Swellable Silk Fibroin Microneedles for Transdermal Drug Delivery

Zhuping Yin[1], Dajiang Kuang[1], Shiyi Wang[1], Zhaozhu Zheng[1], Vamsi K. Yadavalli[2],

Shenzhou Lu[1]*

[1]National Engineering Laboratory for Modern Silk, College of Textile and Clothing Engineering, Soochow University, Suzhou 215123, People's Republic of China

[2] Department of Chemical & Life Science Engineering, Virginia Commonwealth University, Virginia 23284-3028, USA

*Corresponding author:

Shenzhou Lu

Telephone: +86 512-67061152

e-mail: lushenzhou@suda.edu.cn

GRAPHICAL ABSTRACT

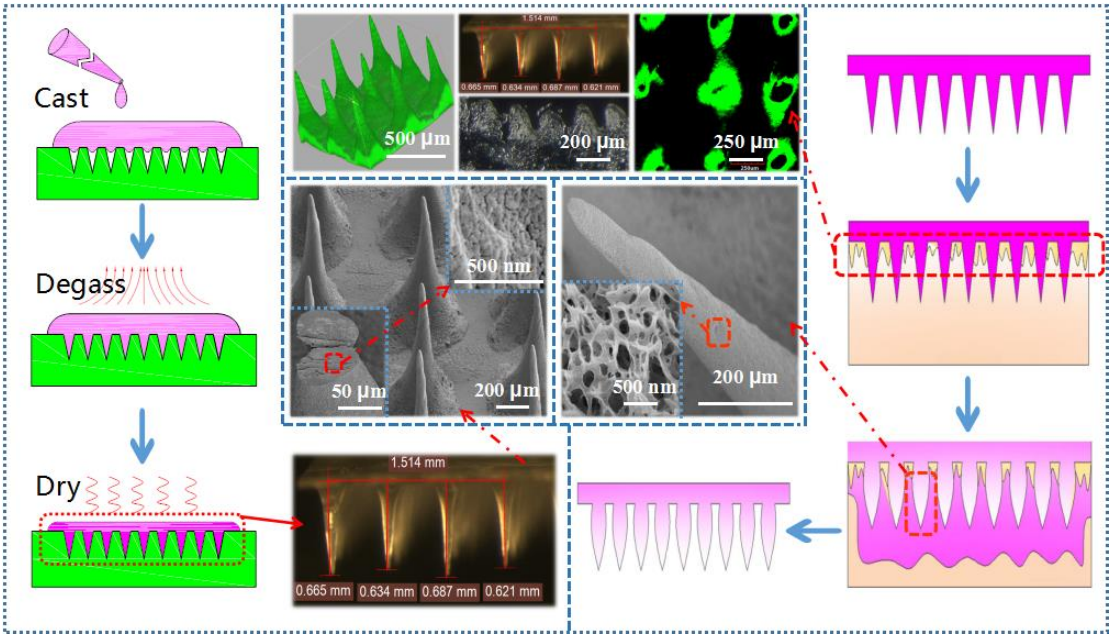

Statement of Significance

This study demonstrate (1) a novel swell-to-release silk fibroin (SF) micromeedle system for transdermal drug delivery, in which the swelling modified SF microneedles (MNs) can effortlessly pierce human epidermal skin in its dried state and swell into a a semi-solid, acerose hydrogel with a controlled 3-dimensional (3D) porous network structure inside for a controllable transdermal drug delivery; (2) different micromolecular reagents were mixed with SF to make the SF composite swellable and insoluble; (3) 2-ethoxyethanol (ECS) modified SF microneedles can easily pierce porcine skin with a depth of ~200 μm in vitro, and transform into semi-solid hydrogels with 50 - 700 nm porous network inside; (4) the swelling modified SF MNs exhibit more consistent and controllable drug releasing capacities than those of dissolving MNs; (5) the better swelling capacity of the microneedles produces the larger swelling pores inside, in accordance with the higher transdermal drug release kinetics and final accumulative releasing ratio.

Abstract: In this paper, a swelling-modified silk fibroin (SF) microneedle for transdermal drug delivery is presented. The microneedles undergo a phase transition from a dried and

rigid state to a semi-solid, acerose hydrogel state with a controlled 3-dimensional (3D) porous network structure. Different micromolecular reagents have been studied for mixing with aqueous silk fibroin to endow a swellable and insoluble capacity to the SF. The aqueous SF composite is poured on a polydimethylsiloxane (PDMS) mold with arranged micropores on its surface to fabricate SF microneedles with high fidelity and mechanical robustness. The results demonstrate that 2-ethoxyethanol (ECS) modified SF microneedles can easily pierce porcine skin with a depth of ~200 μm *in vitro,* and transform into semi-solid hydrogels with 50 - 700 nm porous network inside. These swelling-modified microneedles can accomplish a significantly enhanced transdermal drug release capacity in proportion to their swelling characteristics. The better swelling capacity of the microneedles produces larger pores, resulting in higher transdermal drug release kinetics. There is also a relationship between swollen pore dimensions and the molecular weights of encapsulated therapeutics. The controllable properties of these SF microneedles coupled with their high biocompatibility, render swell-to-release ECS/SF composites as viable transdermal delivery devices.

Keywords: silk fibroin; microneedle; hydrogel

1. Introduction

Transdermal drug delivery systems (TDDS) have been widely used to transport medications owing to their features, including ease in controlling levels in plasma, safe administration, favorable patient compliance due to avoidance of palatability issues, and evading hepatic/gastrointestinal metabolism compared with oral therapeutics [1]. However, the outermost *stratum corneum* of skin with a thickness of 10 - 15 μm that forms a natural barrier preventing the interstitial surroundings *in vivo* from outside invasion, also provides the major obstacle for transdermal drug delivery, especially for macromolecular bioactive diffusion [2-4]. Researchers have reported several approaches, including ultrasound, electric fields, chemical enhancers, and thermal methods to enhance percutaneous therapeutic diffusion [5]. Nevertheless, the effective transdermal diffusion of macromolecular agents still remains an unsolved challenge [6].

In recent decades, microneedle-based TDDS (MTDDS) formed by fabricating reversible solid microchannels for bioactive diffusion have drawn much attention, and been widely explored due to their safety, minimal invasiveness, and high therapeutic efficacy [6-8]. Microneedle systems (MNS) are usually composed of a basal layer and dozens to hundreds of micro-projections, perpendicularly attached to the surface. These range in height from 100 - 1000 μm and come in different shapes and tip-to-tip intervals [6,9]. Compared to conventional TDDS, the MTDDS can significantly enhance transdermal drug permeation by producing solid, yet reversible hollows inside the corneum [10], the outermost barrier of the epidermis. This makes MTDDS extremely suitable for the transdermal permeation of macromolecular

therapeutics sensitive to enzymatic or acidic degradation within the gastrointestinal tract, especially vaccines [11-12], insulin [10,13], antigens [14], DNA and RNA bioagents [15]. The MTDDS can be easily self-administered and significantly, facilitate percutaneous penetration with minimal pain and tissue damage because of their micro-sized dimensions [10]. In addition, microneedle systems can be easily removed, and offer better control of therapeutic levels, further resulting in proper patient compliance [16-17].

Despite the many advances and diverse types of microneedles available (solid, coated, hollow and dissolving MNS) [11], there remain several technical bottlenecks in practical applications. These include complicated and high-cost processing, often poor biocompatibility of the base materials, and difficulty of controlling the rate of transdermal drug delivery [18-19]. Metal, glass or silicon microneedles can easily penetrate human epidermal tissue due to their inherent stiffness. However, inevitable needle fractures and non-degradable residues after the administration of these MNS result in long-lasting irritation and sensitization to skin. Moreover, the low dose of coated drugs limits practical uses, especially for long-term applications [20-21]. The use of adaptive, biocompatible materials to fabricate MNS can address some of these issues.

Hydrogels are biocompatible polymers with a three-dimensional (3D) porous structure that can swell in water and release loaded agents via free diffusion, and form ideal vehicles for transdermal drug delivery [21-24]. Conversely, hydrogels lack the mechanical strength required to penetrate the epidermis. The versatile silk fibroin (SF) with its biocompatibility, controllable degradability, and excellent mechanical properties, is extremely suitable as the

base material for microneedles [25-26]. However, pure SF microneedles are soluble and lead to burst release of loaded drugs, making them unsuitable for long term release [27]. Here, we demonstrate a composite made from micromolecular reagents mixed with aqueous SF to endow a swellable and insoluble capability. The swelling modified SF composite is used as the structural material to form a micro-needle system for controlled transdermal drug delivery. The MNS can easily penetrate epidermal skin in its dry state, and release drugs consistently and controllably after a transition into a polyporous hydrogel. The better swelling capacities of the microneedles create the larger pores thereby resulting in higher transdermal release kinetics. Moreover, there is adaptability between the dimensions of the swollen pores and the molecular weight (MW) of the encapsulated therapeutics, with even stronger release kinetics at higher MW accomplished by enhancing swelling capacity of MNS. The results demonstrate that the swellable silk fibroin MNS perform a more consistent and controllable transdermal drug delivery than those of dissolving SF MNS for several minutes to several hours administration *in vitro* [4,10]. Owing to the controlled swelling-to-release mechanism, and the inherent biocompatibility of fibroin, these swelling modified SF MNS form suitable candidates for a controllable transdermal drug delivery system.

2. Materials and Methods

2.1 Preparation of Silk Fibroin solution

B. mori silkworm cocoons (supplied by Anhui Agricultural University) were degummed three times in 0.5% (w / v) Na_2CO_3 solution at 98 - 100℃ for 30 min, and then washed completely with deionized (DI) water to remove the sericin proteins on the outermost surface.

After thoroughly drying at 60 ºC for at least 6h, the silk fibers were dissolved in LiBr solution (9.3 M) in a 15:100 bath ratio (w/v) for 60 min, followed by dialyzing process against running DI water to remove salts and small molecules using Slide-a-Lyzer dialysis cassettes (Pierce, MWCO 8 - 12 KD) for 3 - 4 days. The silk fibroin was further purified by centrifuging method [18]. Concentration of the final SF solution was above 7.0 % (w/v), measured by weighing the mass before and after drying. All solutions were stored at 4 ºC prior to processing [28-30].

2.2 Fabrication of swelling modified microneedle

Urea (URE), N-dimethylformamidee (DMF), glycine (GLY) and 2-ethoxyethanol (ECS) purchased from Sinopharm Chemical Reagent Co., Ltd were mixed with aqueous silk fibrion at the blending ratio (S) of 0/10, 0.25/10, 0.5/10, 1/10, 2/10 and 3/10 (m_x/m_{SF}) to endow the SF MNS with an insoluble and swellable capacity. The final SF concentration is 6 % (w/v). The modified aqueous silk solution was poured on a polydimethylsiloxane (PDMS) mold with 15 × 15 pore array with 300 - 700 μm depth and 150 - 1000 μm intervals, followed by several degassing steps (> 0.09 MPa) using a vacuum dryer and drying process (25 ºC, 55 % humidity) for 24 h **(Fig. 1-A)**. The features of these obtained microneedles were imaged by using a Leica MZFILL stereomicroscope, scanning electron microscope (SEM) and laser scanning confocal microscopy (LSCM).

2.3 Dissolving and swellable capacity of modified SF MNS

To obtain the SF MNS with consistent and controllable transdermal delivery capacities, characteristics of insolubility and swellability within interstitial fluid after administration are

essential. The modified SF MNS was immersed in PBS (pH = 7.4) to evaluate its dissolving [31] and swelling [32] characteristics. The morphological dimensions of SF MNS before and after swelling were monitored by stereomicroscope and SEM. Dried SF microneedles weighed as m_1 (0.1g) were swollen in 10 mL PBS for 24 h at 37 °C and bath ratio of 1:100 (w/v), 4 parallel samples each group. After centrifuging at 3500 r/min for 15 min, the supernatant was tested by using an ultraviolet spectrophotometer at 278 nm to evaluate the concentration (C_1) of silk fibroin dissolved in PBS. The corresponding residues were weighed (m_2) after drying with filter paper to remove any surface water. The ratio of solid matrix content in MNS (Φ_1) was obtained with a 105 °C drying and weighing procedure to help evaluating the swelling and dissolving characteristics. The percentage swelling and dissolving were calculated, respectively, by using the Eq. 1 and Eq. 2:

$$Swelling\ (\%) = \frac{m_2 - m_1}{m_1 \times \phi_1 \times [1/(1+S)]} \times 100\ \% \quad (1)$$

$$Dissolving\ (\%) = \frac{10 \times C_1}{m_1 \times \phi_1 \times [1/(1+S)]} \times 100\ \% \quad (2)$$

Where m_1 and m_2 are the mass of SF MNS before and after immersion in PBS, Φ_1 is the ratio of solid matrix content in SF MNS, S is the mass ratio between SF and the micromolecular reagents used for swelling modification, and C_1 is the concentration of dissolved SF after immersion in PBS.

2.4 Mechanical characteristic and penetrating capacity of SF MNS

The SF MNS was subjected to a compression test to evaluate its mechanical properties [18]. The MNS (300 μm length), modified with ECS at 0/10, 0.5/10, 1/10 and 3/10 ratios were

tested using a TAXT2 texture analyzer with a 0.02N trigger force and 10 mm/min velocity, 15 parallel samples each group. SF MNS mixed with FITC () was used to puncture porcine and rabbit skin with a homemade applicator *in vitro* to evaluate its practical insertion capacity. Following formalin fixation, the punctured skins and its vertical microsections were imaged with a Leica MZFILL stereomicroscope to evaluate the puncture morphology. LSCM was used to measure the microchannels at different depths inside porcine skins derived from MNS puncturing.

2.5 Conformation and aggregation structure of Modified SF MNS

Fourier transform infrared spectroscopy (FTIR) was used to analyse the conformational structure of the swellable, modified MNS, using a Nicolet 5700 FTIR spectrometer (Nicolet Co., USA) with KBr tabletting. The IR spectra recorded the absorbance of the sample at 400 - 4000 cm^{-1}. X-ray diffraction (XRD) was performed to reveal the aggregation structure of SF MNS using an X-ray diffractometer (X0 Pert-Pro MPD, PANalytical, Almelo, Holland) with CuKa radiation. The XRD patterns were recorded in the range of 2θ from 5° - 45° at a 10°/min, 35 mA and 40 KV. Fourier self-deconvolution of IR spectra in the amide I region (1595 - 1705 cm^{-1}) was performed using Peakfit to evaluate secondary structure content [33]. Deconvolution was performed using a Gauss algorithm with a smoothing and amp value of 1.0 % and 1.5 %. FTIR spectra were curve-fitted to measure the original areas of each amide I region [34].

2.6 Enzymatic degradation of modified SF MNS in vitro

SF MNS were immersed in PBS (37 ^{o}C, pH: 7.4) containing protease XIV (2 U/ml,

Sigma-Aldrich) and collagenase I (2 U/ml, Sigma-Aldrich) at a bath ratio of 1/100 (w/v). The solution for degradation was renewed daily. SF peptide content derived from enzymatic degradation was measured by sampling at designated time points, 4 parallel samples each group [34]. Percentage enzymatic SF degradation was calculated using Eq. 2 mentioned above.

2.7 Transdermal delivery of FITC-dextran in Vitro

To assess the transdermal delivery characteristics of the swelling modified MNS, various dextrans tagged with fluorescein isothiocyanate isomer I (FITC-Dextran, Mw: 5 kDa, 10 kDa, 40 kDa, purchased from Xi"an Ruixi Biological Technology Co., Ltd) were used as the model agents at the ratio of 1/20 ($\Psi = m_{FITC\text{-}Dextran} / m_{SF}$). The ECS modified MNS with swelling ratio of 300, 500 and 700 %, and the dissolving pure SF MNS were administered for transdermal diffusion *in vitro*, with the corresponding drug loaded SF films as the control groups. The drug loaded MNS were applied on pig cadaver skin with a 500 - 600 μm thickness using a homemade applicator *in vitro*, followed by fixation to a TT-8 transdermal diffusion apparatus in 32 ºC PBS (pH: 7.4, V = 13 ml) (**Fig. 1-B**) [35], 4 parallel samples each group. All the releasing groups were sampled regularly at time points established before, followed by fluorescence detection to monitor the concentration (C_i) of FITC-Dextran from the transdermal release using a FM4P-TCSPC fluorescence spectrometry analyser, with a 495 nm excitation wavelength and 516 nm emission wavelength. The percentage drug release was calculated using Eq. 3:

$$Accumulating\ (\%) = \frac{C_n \times V + \sum_{i=1}^{n-1} (C_i \times V_i)}{m_1 \times \phi_1 \times [\psi / (1 + \psi + S)]}, \quad (n = 2,3,4\cdots) \tag{3}$$

Where C_i is the FITC-Dextran concentration in PBS transdermal release from MNS, i is the sampling time, V_i is the sampling volume (1 ml), Ψ is the mass ratio between SF and FITC-Dextran, Φ_1 is the ratio of solid matrix content in SF MNS, and S is the mass ratio between SF and the reagents used to swelling modification.

Fig. 1. Schematic of the swelling-to-release MNS.

3. Results

3.1 Fabrication of Swelling Modified SF MNS

To investigate the feasibility for fabricating swelling-modified SF MNS for transdermal delivery, the modified aqueous SF solution mixed with FITC-Dextrans of different sizes (MW: 5 kDa, 10 kDa, 40 kDa) at a ratio of 1/20 ($m_{FITC\text{-}Dextran}/m_{SF}$) was poured on a PDMS mold with different micropore depth sizes (300 - 700 μm) and tip-to-tip intervals (600 - 1000 μm). Using this approach, a mechanically tough and solid MNS with encapsulated FITC-Dextran was successfully obtained from the PDMS molds after several degassing and drying steps at 25 ºC and 65 % humidity (**Fig. 1-A**). The obtained SF microneedles with various needle heights and tip-to-tip intervals but identical piniform shapes were measured with stereomicroscope, SEM (**Fig. 2**). The layer scanning technique in SCLM was used to image 3D structures/dimensions of the obtained MNS (**Fig. 2-C$_3$ and D$_3$**). The results indicate that the MNS can be produced repeatedly and share identical piniform morphology derived from the predesignated micropores inside the PDMS molds.

Fig. 2. Morphology of MNS with different dimensions.

3.2. Dissolving and swelling capacity of modified SF MNS

To function as a "swell-to-release" MTDDS, the MNS should not only possess proper mechanical characteristics, but also be minimally dissolving and highly swellable *in vivo* for controlled release. Thus, the MNS can easily puncture the human epidermis in its dry state, while swelling into hydrogels with minimal dissolution by absorption of interstitial fluid. Herein, we fabricated the swelling-modified SF MNS by blending SF and micromolecular reagents using the approach mentioned above, followed by dissolution and swelling measurements (pH: 7.4, 37 ^{o}C, 24 h). The results indicate that pure SF MNS shows a robust dissolving characteristic *in vitro* with nearly 50 % mass loss after a 24h immersion in PBS (**Fig. 3-A**). In contrast, the modified SF MNS display a significant decrease in their dissolution characteristics with increasing usage of these micromolecules. For instance, even minimal quantities of GLY and URE can easily make the SF MNS nearly insoluble (< 10 %), corresponding to a significantly decreasing swellable capacity (< 200 %). ECS and DMF endow the SF MNS with both a decreasing dissolution and a significantly higher swelling capacity. In particular, the ECS/SF blending MNS exhibits a minimal dissolution (< 10 %) together with an extraordinary swelling characteristic (> 500%) at the ECS/SF (w/w) mixing ratio of 1/10. A significant increase in morphological size and 3D porous network morphology is also observed (**Fig. 3-B** and **Fig. 4**). Therefore, the ECS/SF formula was noted to be preferred and further researched herein.

Fig. 3. Swelling and dissolving characteristics of modified SF MNS (PBS, pH: 7.4, 37℃, 24 h).

The swelling-modified SF MNS display controllable transdermal release by absorbing interstitial fluid, and transforming into hydrogels with controllable 3D porous network structures. The swelling ratio dependence of the 3D network and pore dimensions inside the ECS-modified SF MNS was measured by SEM (**Fig. 4**). In the dry state, the MNS has an extremely closely-stacked aggregate structure with less microscopic pores and minimal pore size (< 10 nm, **Fig. 4-A**), corresponding to a robust mechanical strength and penetration ability. In contrast, pure SF MNS dissolves rapidly upon penetrating porcine skin *in vitro*, resulting in the disappearance of mesoscale needles arranged on the base support, and the appearance of micelle morphology derived from self-assembly of the dissolving SF (**Fig. 4-B**). Notably, the swelling-modified SF MNS possess an extraordinary and controllable 3D porous network morphology with pore dimensions in positive proportion to the swelling capacity (or swelling ratio). The swelling-modified SF MNS with a 200 - 700 nm microscopic pore size attains a 650 % swelling ratio (**Fig. 4-C**) after PBS immersion. The 3D porous network morphology of modified SF MNS with a 50 - 400 nm pore size range exhibits a 500 % swelling ratio (**Fig. 4-D**). The SF MNS with a 50 - 100 nm pore size displays a 250 % swelling ratio (**Fig. 4-E**) in PBS. Thus, the 3D porous network dimensions inside swelled MNS can be controlled by simply adjusting the ECS/SF blending ratio.

Fig. 4. SEM morphology of swelled SF MNS after immersion (PBS, pH: 7.4, 37 ℃, 24 h).

3.3 Mechanical analysis and degradation characteristic of ECS modified MNS

To evaluate the capacity for skin insertion as well as the bulk mechanical characteristics of swelling-modified SF MNS, the fabricated microneedles were penetrated into porcine skin *in vitro,* and the compressive strength measured using a TAXT2 texture analyzer. The results derived from the compression test indicate that all the SF MNS perform more than 0.25 N/needle compressive fracture force, which is adequate for skin insertion [36]. There is a minimal enhancement of mechanical properties with increased ECS/SF blending ratio, despite a statistically insignificant ANOVA (**Fig. 5-A** and **B**). SF MNS with a length of ~ 500 μm and encapsulated FITC-dextran was inserted into porcine and rabbit skins using a homemade applicator to evaluate insertion capacity *in vitro* (**Fig. 5-C**). A histological examination shows that SF MNS can effortlessly penetrate porcine and rabbit skins (**Fig. 5-D**) *in vitro,* and result in solid microchannel array with a depth of ~200 μm (**Fig. 5-D$_4$**) on the skin surface. LSCM was also used to measure the microchannels resulting from MNS insertion at different depths. Finally, the images of solid microchannels in different depths were synthesized into a 3D solid microchannel array along the direction of penetration of the MNS (**Fig. 5-E**). These results show that the swelling-modified SF MNS is indeed mechanically tough enough to penetrate into the epidermis of skin, and result in solid microchannels on the skin surface for transdermal drug delivery.

The enzymatic degradation *in vitro* was used to access the degradation capacity of these

swelling-modified SF MNS. PBS (pH = 7.4, 37 ^{o}C) containing collagenase I and protease XIV (2 U/ml) were used as the aqueous surroundings to mimic interstitial fluid for degradation of modified MNS *in vitro*. The SF MNS shows controllable degradation kinetics negatively correlated to the ECS/SF blending ratio. There is a greater than 65 % mass loss of swelling modified MNS (ECS/SF: 0.5/10) within 10 days in the presence of protease XIV. These results show the modified SF MNS as a potentially biodegradable transdermal delivery system that also have the potential to avoid long-lasting irritation and sensitization to skin.

Fig. 5. Mechanical characteristics and insertion capacity of swelling-modified SF MNS.

3.4 Conformation and aggregation structure of Modified SF MNS

Unlike currently available insoluble, non-swelling MNS, and rapidly dissolving polymer MNS, the swelling-modified SF MNS can swell into a porous hydrogel with minimal dissolution upon contact with interstitial fluid. To understand the mechanisms for this unique behavior, FTIR and XRD were used to reveal the conformation and aggregation structure of SF MNS. Normal pure SF MNS shows several IR absorption peaks at 1647 cm^{-1} (amide I), 1642 cm^{-1} (amide II), 1235 cm^{-1} (amide III) and a widespread peak in XRD curves, which is typical of random coil conformers and major amorphous aggregation structure [33-34,37-38], corresponding to a significant dissolving characteristic (**Fig. 6**). DMF, GLY and URE modified MNS exhibit a significantly decreasing dissolving and non-swelling characteristics with its increasing usages, corresponding to relative sharp IR absorption peaks at 1686 cm^{-1}

(amide I), 1625 cm^{-1} (amide II), 1647 cm^{-1} (amide I), 1542 cm^{-1} (amide II), 1525 cm^{-1} (amide I) and 1235 cm^{-1} (amide III) and significant typical silk I crystal peaks at 12.2 °, 19.7 °, 28.2 °, 32.3 °, 36.8 ° and a minimal silk II crystal peak at 20.7 ° in XRD, which are representative of corner, β-sheet, random coil conformers and a significant silk I crystal aggregation structures [33-34,37-38]. The higher the concentration of DMF, GLE or URE, the more significant corner, β-sheet conformers and silk I crystal aggregation structure, the lower the dissolving and swelling characteristic (**Fig. 6 - B - D**).

In comparison, ECS modified SF MNS display relatively weak IR absorption peaks at 1686 cm^{-1} (amide I), 1625 cm^{-1} (amide I), 1647 cm^{-1} (amide I), 1542 cm^{-1} (amide II), 1525 cm^{-1} (amide I) and 1235 cm^{-1} (amide III). Minimal silk I crystal peaks at 12.2 °, 19.7 °, 28.2 ° and negligible silk II crystal peak at 20.7 ° in XRD curves (**Fig. 6-A_1 - A_2**) are observed, corresponding to a significantly decreasing dissolving, but high swelling capacity. To uncover the mechanism of the insoluble and swellable characteristics of ECS modified SF MNS, Fourier self-deconvolution of the IR spectra in amide I (1595 - 1705 cm^{-1}) was conducted using Peakfit v4.12 to specifically evaluate secondary structure content (**Fig. 6-A_3**). The results demonstrate that there is a remarkable conformational transition from random coil conformer to corner, and β-sheet conformers with increasing ECS usage. Hence, it is presumed that the random coil, corner and β-sheet conformers' content of SF polymer play essential roles in contributing to the insolubility and swellability of these SF composites. It may be noted that, compared with GLY, URE, DMF-modified SF MNS, the ECS modified groups show less β-sheet, corner conformers and silk I crystal aggregation structures at the

blending ratio of 0.5/10 and 1/10, in accordance with more random coil conformers and amorphous aggregation structures (**Fig. 6-A$_3$**, **Figure S1**), which form the basis for the insoluble and swellable characteristics.

Fig. 6. Blending ratio (m_X/m_{SF}) dependence of conformation and aggregation structure of swelling-modified SF MNS evaluated by FTIR and XRD.

3.5 Transdermal drug delivery in vitro

Transdermal delivery of modified SF microneedles with different swelling capacities were studied *in vitro* to evaluate the swelling-to-release profiles. FITC-dextrans with different molecular weights (MW) were used as the model therapeutics to clarify the adaptability between therapeutic MW and MNS swelling capacity which can further reveal the swelling-to-release mechanism. Identical, swelling-modified SF films with encapsulated FITC-dextrans were used as control groups to highlight the enhanced transdermal drug delivery derived from microneedle systems. The SF MNS display a significantly enhanced transdermal drug release kinetics compared with the controlled SF films, with 2 - 10 times larger accumulative release ratio than the corresponding control groups during the entire release process (**Fig. 7**). The release profiles show that there are relatively more consistent transdermal drug delivery processes observed 50 - 60 hours after administration of swelling-modified SF MNS, in comparison to the dissolving MNS which make an exhaustive release within 16 hours (**Fig. 7-A**). The dissolving pure SF MNS exhibit significantly

stronger release kinetics compared with the swelling-modified ones in each molecule weight group. In particular, there is an almost 100 % percutaneous release ratio within 16 h in minimal FITC-Dextran molecular weighted group (**Fig. 7-A**). An increase in transdermal drug releasing kinetics of swelling-modified MNS is observed with increase in swelling capacity, similar to the trend in swelling-modified SF films. The lower the ECS/SF blending ratio of MNS, the higher the swelling ratio and corresponding release kinetics. The transdermal release kinetics were measured quantitatively using the linear fitting slope of swelling-modified MNS transdermal release profiles within 12 hours (**Fig. 7 - C**). The results demonstrate that the releasing profiles in better swelling systems are always sharper than those of less swelling systems (**Fig. 7-D**). It is worth noting that the higher the MNS swelling capacity, the sharper the linear fitting profile and the stronger the release kinetics (**Fig. 7-A - C**), likely resulting from a larger porous structure inside the better swelling MNS (**Fig. 4**).

Fig. 7. Accumulating transdermal drug delivery profiles.

The linear fit of the slope of the MNS transdermal release profiles were analyzed (**Fig. 7-A-C)** and contrasted to reveal the mechanism of swelling to release (**Fig. 7-D**). The results demonstrate that there is diverse release kinetics in negative proportion to the MW of the encapsulated payload, in all swelling MNS groups. The lower MW therapeutics can diffuse easily into porcine skin, with stronger release kinetics *in vitro*, in comparison to larger MW, derived from a more facile diffusion process inside the 3D porous network structure of

swelled MNS (**Fig. 4**). Notably, the MNS with a swelling ratio of 650% and encapsulated with 40 kDa FITC-Dextran exhibit a significantly higher releasing kinetics than the MNS with a 250% swelling ratio and loaded with 20 kDa FITC-Dextran. This implies that larger MW therapeutics can also accomplish remarkable transdermal release kinetics comparable to those of lower MW therapeutics using this swelling-to-release MNS. Therefore, the porous network dimension of swelled MNS plays a critical role in the transdermal drug delivery process.

4. Discussion

To overcome the limitations of a rapidly dissolving and burst transdermal release in dissolving (unmodified) SF MNS, the ECS/SF blending method was used to make the SF MNS insoluble and swellable. The ECS/SF blended MTDDS with the ability of "swelling-to-release" are used to accomplish controllable transdermal drug delivery. The obtained MNS possess sufficient mechanical strength to easily pierce human skin in the dried state, which results in a minimally invasive solid microchannel array on the skin surface for transdermal drug delivery (**Fig. 5-D** and **E**). The swelling modified SF MNS then transform into a semi-solid hydrogel with controllable 3D porous network structures (**Fig. 4**) by absorbing the interstitial fluid. This is followed by the controlled diffusion of agents embedded within the gelatinous MNS to the subcutaneous tissue (**Fig. 1-C**), by means of the porous 3D network structure inside the swelled SF MNS (**Fig. 4**).

The higher the ECS/SF blending ratio, the more the content of corner, β-sheet conformers and silk I crystal structures in the dried SF polymer, and the lesser the dissolution

characteristics, together with a remarkable swelling capacity (50 - 800 %) (**Fig. 3 and Fig. 6-A**). The resultant SF MNS is tough enough to puncture the outermost *stratum corneum* of skin and then transform into semi-solid hydrogel with a 50 - 700 nm pore size (**Fig. 4**), resulting in a solid microchannel array with a depth of ~200 μm for transdermal permeation of the encapsulated agents (**Fig. 5-D** and **E**). Further, the higher the swelling capacity, the larger the pore dimensions of swelled SF MNS after administration (**Fig. 4**).

The modified SF MNS with different swelling and loading of FITC-dextran were administered *in vitro* to assess their transdermal drug release capacity. The fabricated SF MNS displays 2 - 10 times higher transdermal drug delivery capacity than corresponding SF films with identical loading and swelling capacity (**Fig. 7**). This ability is derived from the resulting solid microchannels that permit transdermal drug diffusion. The FITC-dextran can easily diffuse from inside to outside the gelatinous MNS with better swelling capacity, making the swelling-modified SF MNS display enhanced percutaneous drug delivery kinetics with increased swelling capacity (**Fig. 7**). Thus, the higher the swelling capacity of SF MNS, the larger the pore dimensions of the 3D network structure in swelled SF MNS, and the stronger the transdermal drug release kinetics.

FITC-dextrans with different MW were used as the model agents encapsulated in swelling MNS to characterize transdermal drug release kinetics, as well as the adaptability between MNS swelling and size of therapeutic loaded. Smaller molecules are easier to diffuse in identical swelled MNS porous network structure. As a consequence, the transdermal drug release kinetics are in negative proportion to the MW of agents embedded in the SF MNS.

The smaller the MW of loaded therapeutic, the stronger the kinetics of transdermal drug release. Interestingly, the larger loaded agents can also accomplish a remarkable transdermal diffusion compared to those of the smaller agents using a MNS with better swelling capacity, derived from the "swelling-to-release" mechanism (**Fig. 1-C**). Hence, the swelling modified SF MNS hold a potential for controllable transdermal drug delivery.

5. Conclusion

In summary, the ECS/SF composites demonstrated here to fabricate silk fibroin based microneedle systems (SF MNS) exhibit minimal dissolution, and controllable swelling characteristics. The SF MNS can easily puncture porcine skin in the dried state, and result in a solid microchannel array with a depth of ~200 μm on the skin surface, followed by a swelling to a hydrogel state by absorbing interstitial fluid. There is an enhanced swelling capacity (250 - 800 %) of SF MNS with the decrease of ECS/SF blending ratio (3/10 - 0.25/10), corresponding to an increasing pore dimension (50 - 700 nm) inside the swelled MNS. This results in a stronger transdermal drug releasing kinetic and final accumulative releasing ratio compared with non-swellable MNS, and a relatively more consistent release within the subcutaneous tissue in comparison to dissolving SF MNS. In addition, There is also a relationship between swollen pore dimensions and the molecular weights of encapsulated therapeutics. Larger therapeutic MW can also display analogous transdermal release kinetics and final accumulative release ratios compared to the smaller therapeutics encapsulated by using a better swelling MNS. The controllable drug release characteristics by swelling to release, combined with the high mechanical strength of these biomaterials and

their high biocompatibility make the modified SF MNS a viable alternative to traditional materials for smart transdermal drug delivery.

5. Acknowledgments

The work is supported by National Natural Science Foundation of China (Grant No. 51373114), College Nature Science Research Project of Jiangsu Province, China (Grant No. 15KJA540001), PAPD, and Nature Science Foundation of Jiangsu, China (Grant No. BK20171239).

References

[1] S. Indermun, R. Luttge, Y. E. Choonara, P. Kumar, L.C. du Toit, G. Modi, V. Pillay, J. Controlled Release, 185 (2014) 130-138.

[2] K. Ita, Pharmaceutics, 7 (2015) 90–105.

[3] J.W. Lee, J.H. Park, M.R. Prausnitz, Biomaterials, 2008, 29(13): 2113-2124.

[4] B. Bediz, E. Korkmaz, R. Khilwani, C. Donahue, G. Erdos, L.D. Falo, O.B. Ozdoganlar, Pharm. Res., 31(2014) 117-135.

[5] R.B. Walker, E.W. Smith, Adv. Drug Delivery Rev., 18(1996) 295-301.

[6] S. Marshall, L.J. Sahm, A.C. Moore, Vaccine, 34(2016) 723-734.

[7] H.S. Gill, D.D. Denson, B.A. Burris, M.R. Prausnitz, J. Pain, 24 (2008) 585–594.

[8] S. Marshall, L.J. Sahm, A.C. Moore, Vaccine, 34(2016) 723-734.

[9] R.F. Donnelly, R. Majithiya, T.R.R Singh, D.I.J. Morrow, M.J. Garland, Y.K. Demir, K. Migalska, E. Ryan, D. Gillen, C.J. Scott, A.D. Woolfson, Pharm. Res., 28 (2011) 41-57.

[10] M.H. Ling, M.C. Chen, Acta biomaterialia, 9 (2013) 8952-8961.

[11] Y.C. Kim, J.H. Park, M.R. Prausnitz, Advanced drug delivery reviews, 64 (2012) 1547-1568.

[12] P. Schipper, K. van der Maaden, S. Romeijn, C. Oomens, G. Kersten, W. Jiskoot, J. Bouwstra, J. Controlled Release, 242 (2016) 141-147.

[13] W. Martanto, J.S. Moore, T. Couse, M.R. Prausnitz, J. Controlled Release, 112 (2006)

357–361.

[14] G. Widera, J. Johnson, L. Kim, L. Libiran, K. Nyam, P.E. Daddona, M. Cormier, Vaccine, 24 (2006) 1653–1664.

[15] M. Pearton, C. Allender, K. Brain, A. Anstey, C. Gateley, N. Wilke, A. Morrissey, J. Birchall, Pharm. Res. 25 (2008) 407–416.

[16] J. Freiherr, M. Hallschmid, W.H. Frey II, Y.F. Brünner, C.D. Chapman, C. Hölscher, S. Craft, F.G.D. Felice, C.Benedict, CNS drugs, 27(2013) 505-514.

[17] H.S. Gill, M.R. Prausnitz, J. Controlled Release, 117 (2007) 227-237.

[18] J.Y. Lee, S.H. Park, I.H. Seo, K.J. Lee, W. Ryu, Eur J. Pharm Biopharm, 94 (2015) 11-19.

[19] Sachdeva V, A.K. Banga, Recent patents on drug delivery & formulation, 5(2011) 95-132.

[20] K. Tsioris, W.K. Raja, E.M. Pritchard, B. Panilaitis, D.L. Kaplan, F.G. Omenetto, Adv. Funct. Mater., 22 (2012) 330-335.

[21] X. Hong , Z. Wu, L. Chen , F. Wu, W. Yuan, Nano-Micro Letters, 6 (2014) 191-199.

[22] R.F. Donnelly, M.T.C. McCrudden, A.Z. Alkilani, E. Larrañeta, E. McAlister, A.J. Courtenay, M.C. Kearney, T.R.R. Singh, H.O. McCarthy, V.L. Kett, E.Caffarel-Salvador, S. Al-Zahrani, A.D. Woolfson, PLoS One, 9 (2014) e111547.

[23] E. Eltayib, A.J. Brady, E. Caffarel-Salvador, P. Gonzalez-Vazquez, A.Z. Alkilani, H.O.

McCarthy, J.C. McElnay, R.F. Donnelly, Eur J. Pharm Biopharm, 102 (2016) 123-131.

[24] E. Caffarel-Salvador, A.J. Brady, E. Eltayib, T. Meng, A. Alonso-Vicente, P. Gonzalez-Vazquez, B.M. Torrisi, E.M. Vicente-Perez, K. Mooney, D.S. Jones, S.E.J. Bell, C.P. McCoy, H.O. McCarthy, J.C. McElnay, R.F. Donnelly, PloS one, 10(2015) e0145644.

[25] W.K. Raja, S. MacCorkle, I.M. Diwan, A. Abdurrob, J. Lu, F.G. Omenetto, D.L. Kaplan, Small, 9(2013) 3704-3713.

[26] N. Panda, A. Bissoyi, K. Pramanik, A. Biswas, Mater. Sci. Eng., C, 48 (2015) 521-532.

[27] J. Lee, S.H. Park, I.H. Seo, K.J. Lee, W. Ryu, Eur J. Pharm Biopharm, 94 (2015) 11-19.

[28] A. Matsumoto, J. Chen, A.L. Collette, U.J. Kim, G.H. Altman, P. Cebe, D.L. Kaplan, J. Phys. Chem. B, 110 (2006) 21630-21638.

[29] S. Nagarkar, T. Nicolai, C. Chassenieux, A. Lele, Phys. Chem. Chem. Phys., 12 (2010) 3834-3844.

[30] S. Lu, J. Li, S. Zhang, Z. Yin, T. Xing, D.L. Kaplan, J. Mater. Chem. B, 3 (2015) 2599-2606.

[31] S. Nagarkar, T. Nicolai, C. Chassenieux, A. Lele, Phys. Chem. Chem. Phys., 12 (2010) 3834-3844.

[32] S. Shang, L. Zhu, J. Fan, Carbohydr. Polym., 86 (2011) 462-468.

[33] S. Bai, X. Zhang, Q. Lu, W. Sheng, L. Liu, B. Dong, D.L. Kaplan, H. Zhu, Biomacromolecules, 15 (2014) 3044-3051.

[34] J. Ming, M. Li, Y. Han, Y. Chen, H. Li, B. Zuo, F. Pan, Mater. Sci. Eng., C, 59 (2016) 185-192.

[35] J.G. Hardy, E. Larraneta, R.F. Donnelly, N. McGoldrick, K. Migalska, M.T.C. McCrudden, N.J. Irwin, L. Donnelly, C.P. McCoy, Mol Pharm, 13 (2016) 907-914.

[36] K.J. Lee, S.H. Park, J.Y. Lee, H.C. Joo, E.H. Jang, Y.N. Youn, W.H. Ryu, J. Controlled Release 192 (2014) 174–181

[37] X. Wu, J. Hou, M. Li, J. Wang, D.L. Kaplan, S. Lu, Acta biomaterialia, 8 (2012) 2185-2192.

[38] Z. Gong, Y. Yang, Q. Ren, X. Chen, Z. Shao, Soft matter, 8 (2012) 2875-2883.

Table of contents graphic

Fig. 1. Schematic of the swelling-to-release MNS: A) Processing of swelling modified SF MNS, B) Transdermal drug delivery model of MNS *in vitro*, C) Swelling-to-release process.

Fig. 2. Morphology of MNS with different dimensions: A) SF MNS with 300 μm in height and 600 μm in interval, B) SF MNS with 500 μm in height and 600 μm in interval, C) SF MNS with 900 μm in height and 600 μm in interval, D) SF MNS with 300 μm in height and 1000 μm in interval.

Fig. 3. Swelling and dissolving characteristics of modified SF MNS (PBS, pH: 7.4, 37℃, 24 h): (A) Blending ratio (m_X/m_{SF}) dependence of the swelling and dissolving kinetics in modified MNS, X: ESC (2-methoxyethanol), DMF (N-Dimethylformamidee), GLY (glycine), URE (urea), (B) Morphology of swelling modified SF MNS (m_{ECS}/m_{SF}: 1/10, swelling ratio: 500 %) before and after immersion.

Fig. 4. SEM morphology of swelled SF MNS after immersion (PBS, pH: 7.4, 37 ℃, 24 h): (A) Dried SF MNS, (B) Pure SF MNS, (C) Swelling modified SF MNS (m_{ECS}/m_{SF}: 0.5/10, swelling ratio: 650 %), (D) Swelling modified SF MNS (m_{ECS}/m_{SF}: 1.0/10, swelling ratio: 500 %), (E) Swelling modified SF MNS (m_{ECS}/m_{SF}: 3.0/10, swelling ratio: 250 %).

Fig. 5. Mechanical characteristics and insertion capacity of swelling-modified SF MNS: (A) Compressive fracture force, (B) Morphology before and after a compression test, (C) Compressive mold used for penetrating *in vitro*, (D) Morphology of solid microchannels on skin surface resulting from penetration *in vitro* monitored by an optical stereomicroscope, (E) Morphology of solid microchannels on skin surface resulting from penetration *in vitro*

monitored by LSCM, (F) Enzymatic degradation of modified MNS in vitro, ① and ④ m_{ECS}/m_{SF} = 3/10, ③ and ⑥ m_{ECS}/m_{SF} = 1/10, ② and ⑤ m_{ECS}/m_{SF} = 0.5/10.

Fig. 6. Blending ratio (m_X/m_{SF}) dependence of conformation and aggregation structure of swelling-modified SF MNS evaluated by FTIR and XRD: (A_1 - A_3) ECS modified MNS, (B_1 - B_2) DMF modified MNS, (C_1 - C_2) GLY modified MNS, (D) URE modified MNS, X: ECS, DMF, GLY and URE.

Fig. 7. Accumulating transdermal drug delivery profile: (A) ECS modified SF MNS with swelling ratio of 650 %, (B) ECS modified SF MNS with swelling ratio of 500 %, (C) ECS modified SF MNS with swelling ratio of 250 %, (D) Summary of transdermal release kinetics for MNS with different swelling capacity and encapsulated with varied molecule weights of therapeutics.

Figure S1. Conformation content derived from FITR spectra: (A) DMF/SF, (B) GLY/SF, (C) URE/SF.

Fig. 1

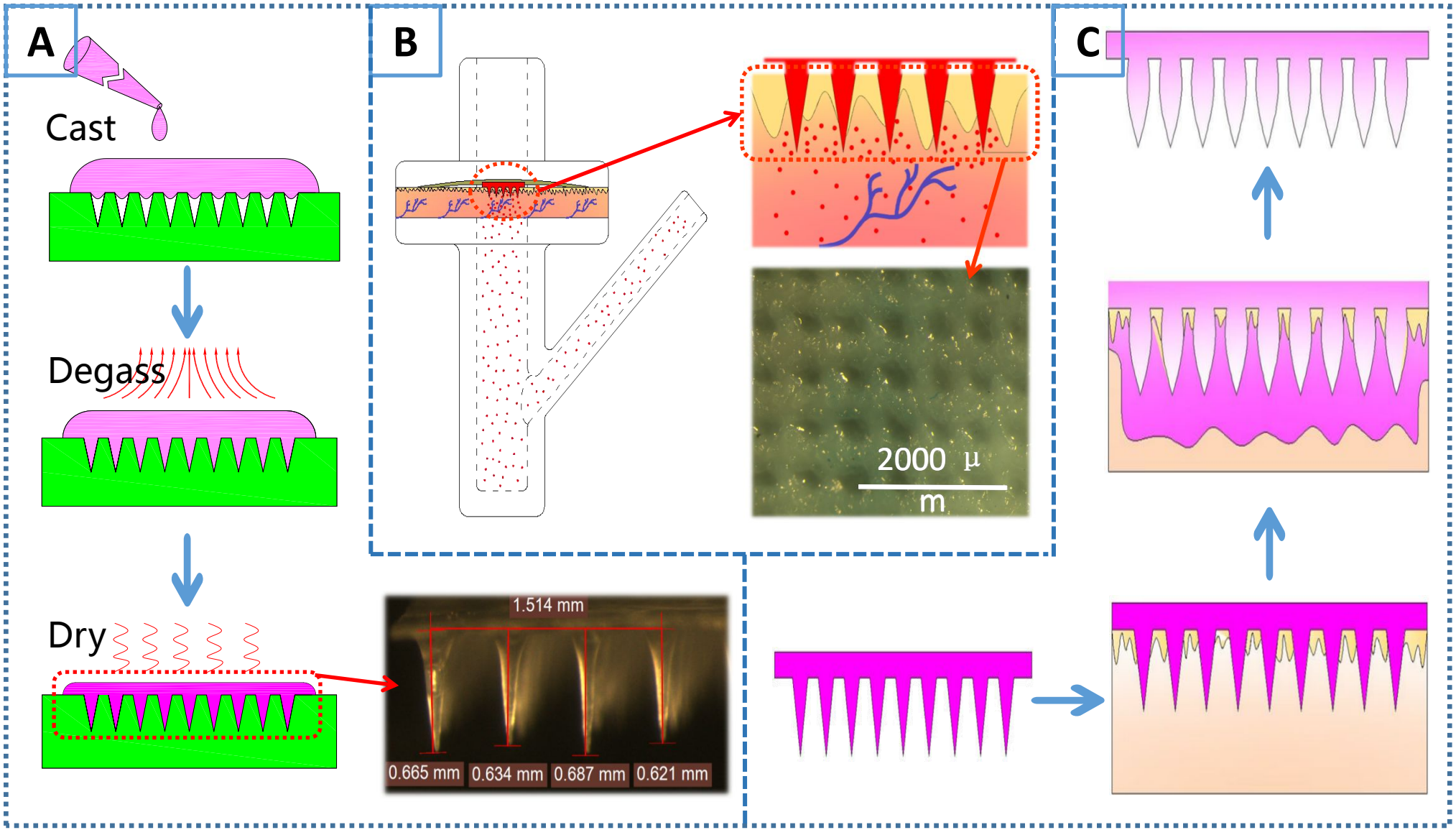
A
Cast
Degass
Dry
B
2000 μ
m
1.514 mm
0.665 mm
0.634 mm
0.687 mm
0.621 mm
C

Fig. 2

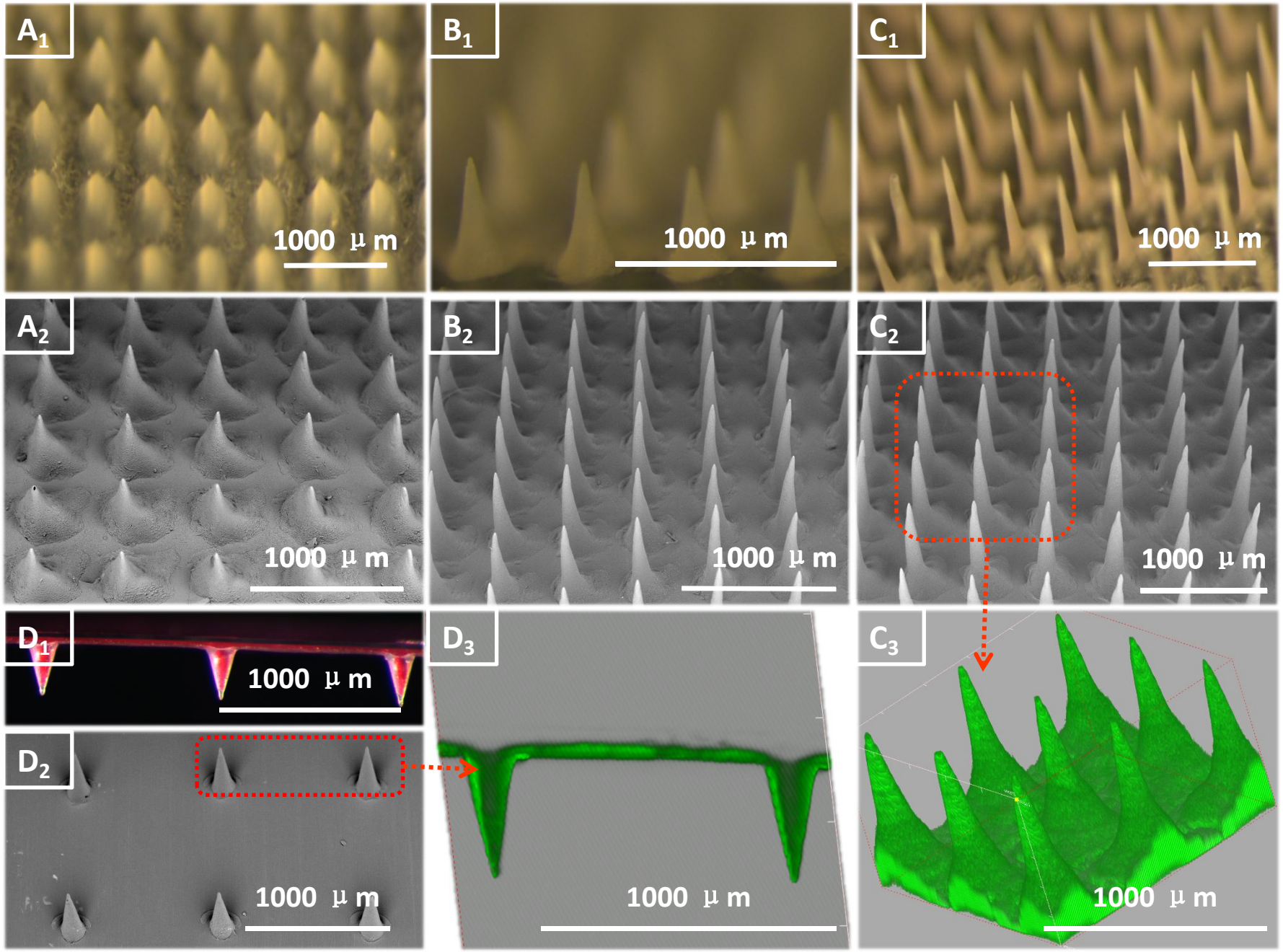
A1
1000 µm
B1
1000 µm
C1
1000 µm
A2
1000 µm
B2
1000 µm
C2
1000 µm
D1
1000 µm
D2
1000 µm
D3
1000 µm
C3
1000 µm

Fig. 3

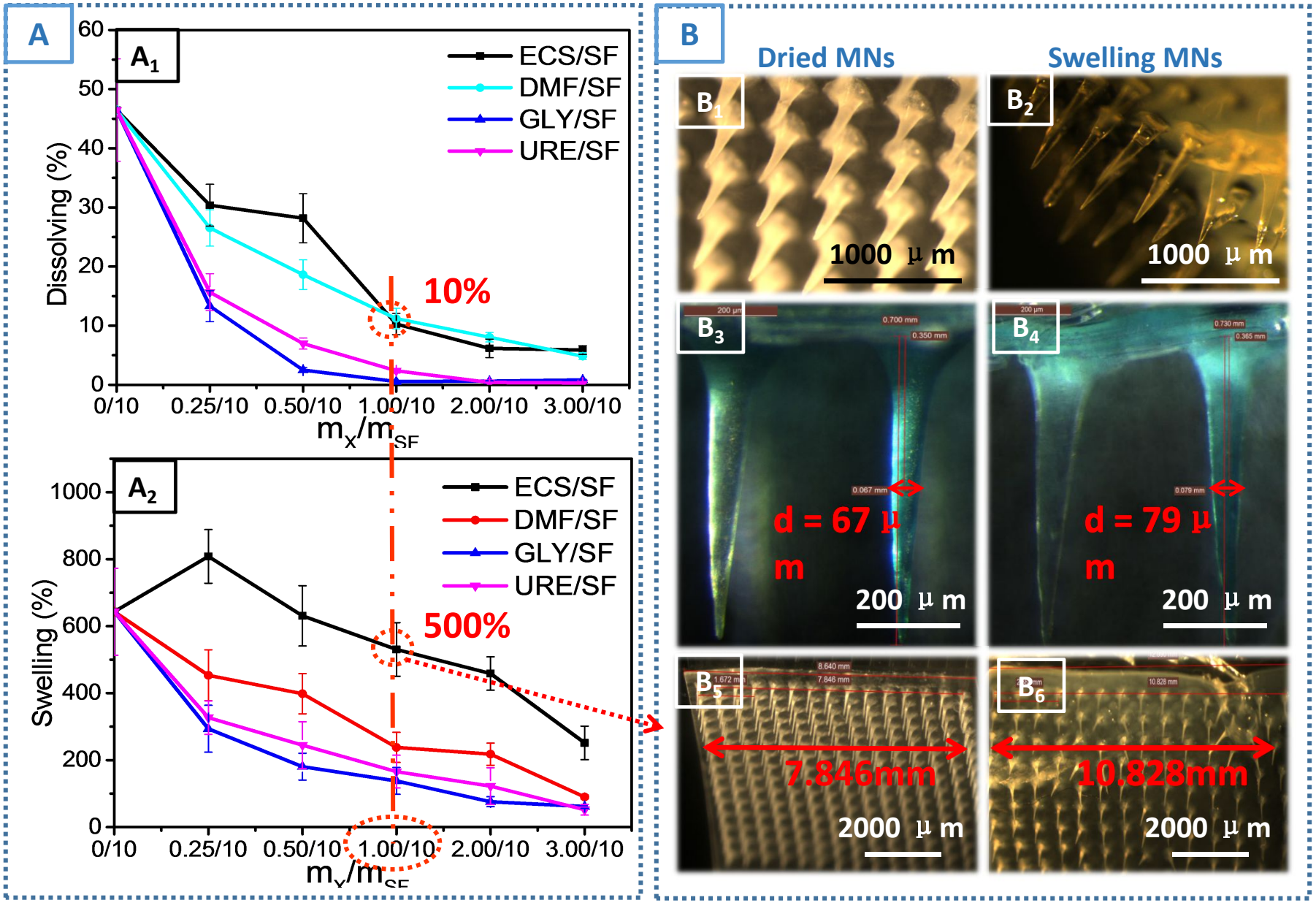
A
A1
ECS/SF
DMF/SF
GLY/SF
URE/SF
Dissolving (%)
10%
0/10
0.25/10
0.50/10
1.00/10
2.00/10
3.00/10
mx/mSF
A2
Swelling (%)
500%
B
Dried MNs
Swelling MNs
B1
B2
1000 μm
B3
B4
d = 67 μm
d = 79 μm
200 μm
B5
B6
7.846mm
10.828mm
2000 μm

Fig. 4

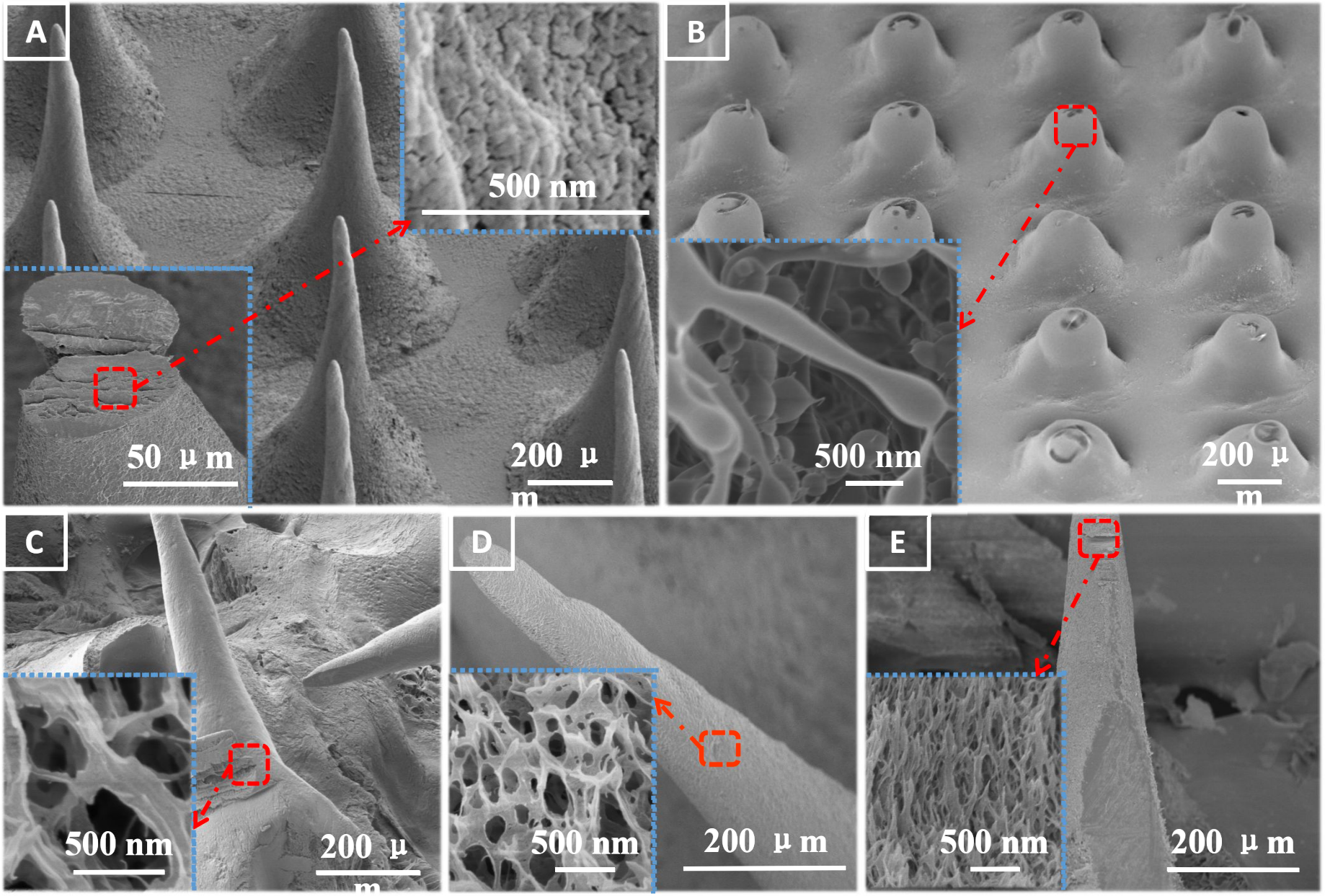
A
500 nm
50 µm
200 µm
B
500 nm
200 µm
C
500 nm
200 µm
D
500 nm
200 µm
E
500 nm
200 µm

Fig. 5

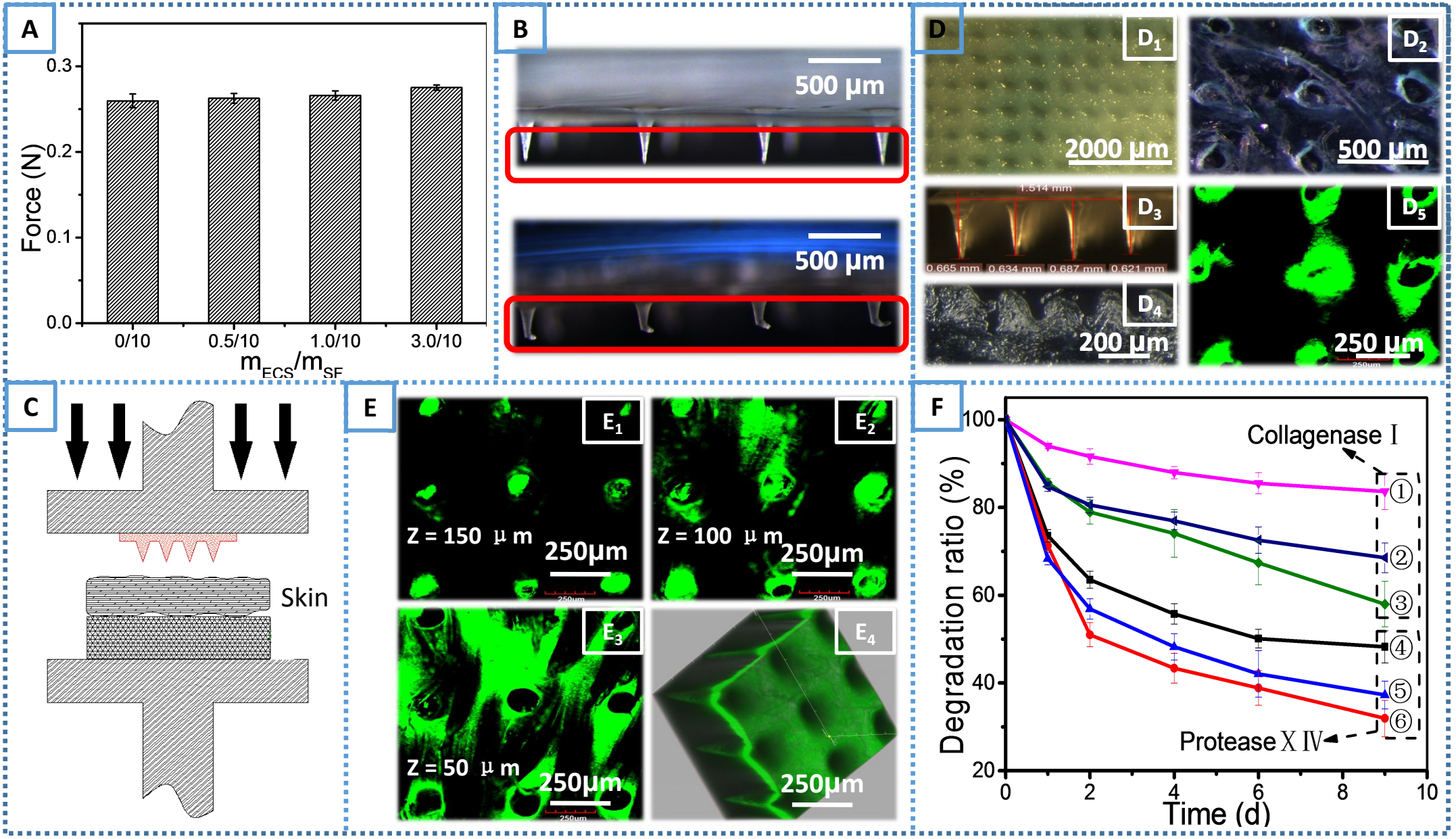
A
Force (N)
0.0
0.1
0.2
0.3
0/10
0.5/10
1.0/10
3.0/10
m_{ECS}/m_{SF}
B
500 μm
500 μm
D
D_1
2000 μm
D_2
500 μm
1.514 mm
D_3
0.665 mm 0.634 mm 0.687 mm 0.621 mm
D_4
200 μm
D_5
250 μm
C
Skin
E
E_1
Z = 150 μm
250μm
E_2
Z = 100 μm
250μm
E_3
Z = 50 μm
250μm
E_4
250μm
F
Degradation ratio (%)
100
80
60
40
20
0
2
4
6
8
10
Time (d)
Collagenase Ⅰ
Protease XⅣ
①
②
③
④
⑤
⑥

Fig. 6

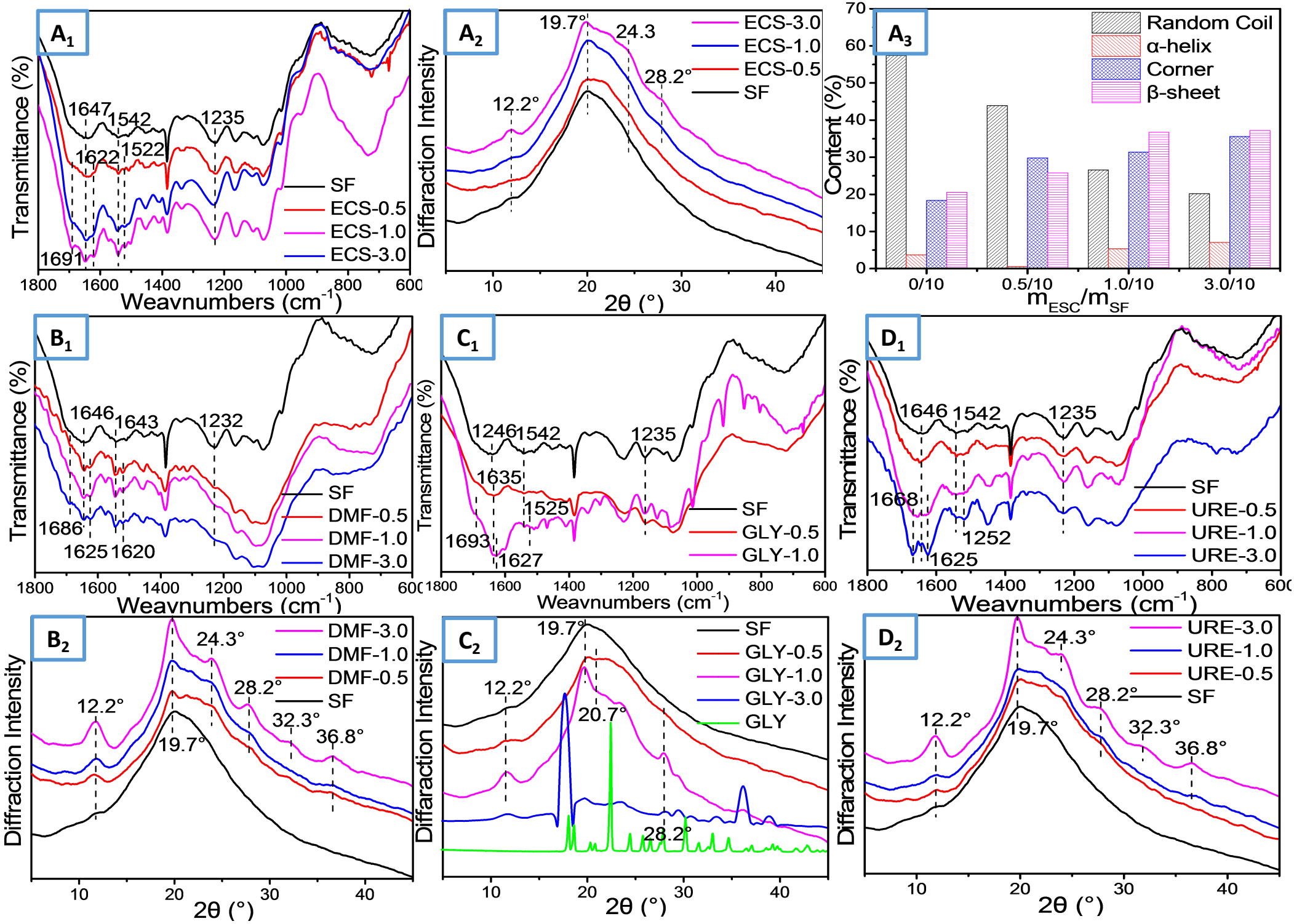
A1
Transmittance (%)
1647
1542
1622
1522
1235
1691
SF
ECS-0.5
ECS-1.0
ECS-3.0
Weavnumbers (cm-1)
A2
Diffraction Intensity
19.7°
24.3
28.2°
12.2°
ECS-3.0
ECS-1.0
ECS-0.5
SF
2θ (°)
A3
Content (%)
Random Coil
α-helix
Corner
β-sheet
0/10
0.5/10
1.0/10
3.0/10
mESC/mSF
B1
Transmittance (%)
1646
1643
1232
1686
1625
1620
SF
DMF-0.5
DMF-1.0
DMF-3.0
Weavnumbers (cm-1)
C1
Transmittance (%)
1246
1542
1235
1635
1525
1693
1627
SF
GLY-0.5
GLY-1.0
Weavnumbers (cm-1)
D1
Transmittance (%)
1646
1542
1235
1668
1252
1625
SF
URE-0.5
URE-1.0
URE-3.0
Weavnumbers (cm-1)
B2
Diffraction Intensity
24.3°
28.2°
12.2°
32.3°
36.8°
19.7°
DMF-3.0
DMF-1.0
DMF-0.5
SF
2θ (°)
C2
Diffraction Intensity
19.7°
12.2°
20.7°
28.2°
SF
GLY-0.5
GLY-1.0
GLY-3.0
GLY
2θ (°)
D2
Diffraction Intensity
24.3°
28.2°
12.2°
19.7°
32.3°
36.8°
URE-3.0
URE-1.0
URE-0.5
SF
2θ (°)

Fig. 7

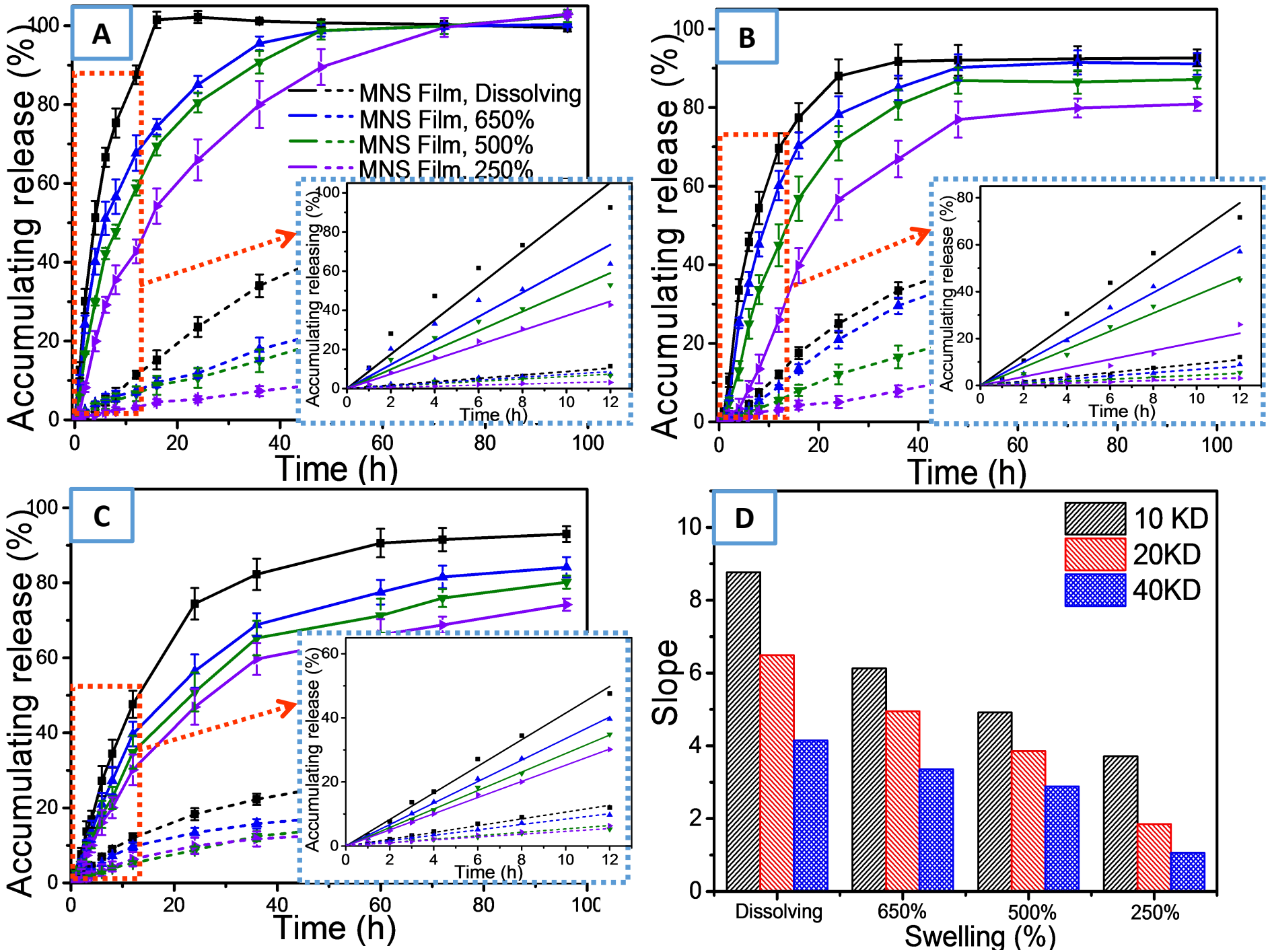
A
Accumulating release (%)
Time (h)
MNS Film, Dissolving
MNS Film, 650%
MNS Film, 500%
MNS Film, 250%
Accumulating releasing (%)
Time (h)
B
Accumulating release (%)
Time (h)
Accumulating release (%)
Time (h)
C
Accumulating release (%)
Time (h)
Accumulating release (%)
Time (h)
D
Slope
10 KD
20KD
40KD
Dissolving
650%
500%
250%
Swelling (%)